TURBULENCE TOPOLOGIES PREDICTED USING A DYNAMIC NON-LINEAR SUBGRID-SCALE MODEL BASED ON SPEZIALE'S QUADRATIC CONSTITUTIVE RELATION

Bing-Chen Wang[1], Jing Yin[2], Eugene Yee[1], and Donald J. Bergstrom[2]
[1]Defence R & D Canada – Suffield,
P.O. Box 4000, Medicine Hat, AB, T1A 8K6, Canada
bingchen.wang@drdc-rddc.gc.ca, eugene.yee@drdc-rddc.gc.ca

[2]Dept. of Mechanical Engineering, Univ. of Saskatchewan,
Saskatoon, S7N 5A9, SK, Canada
jiy080@mail.usask.ca, don_bergstrom@engr.usask.ca

ABSTRACT

Turbulence topologies related to the invariants of the resolved velocity gradient and strain rate tensors are studied. The *a posteriori* large-eddy simulation (LES) approach adopted in this research is based on a dynamic non-linear subgrid-scale model. In contrast to most of the previous research which focussed on only isotropic turbulence, the present study examines the influence of near-wall anisotropy on flow topologies. Some interesting phenomenological results have been obtained including a wing-shaped contour pattern for the marginal expectation of the resolved enstrophy generation and the negative shift of the peak location (mode) in the joint probability density function (JPDF) of invariants of the resolved rate of strain tensor. The newly observed turbulence phenomenologies are believed to be important and efforts have been made to explain them on an analytical basis.

INTRODUCTION

The past decade has seen a rapid development in the methodology of turbulence topology since the seminal works of Chong *et al.* (1990) and Chen *et al.* (1990). This methodology has provided new insight into turbulence phenomena. It is based on analysis of tensorial invariants and utilizes critical-point theory to classify eddying motions (Perry and Chong, 1987). The method of turbulence topology has been developed through theoretical analysis based on restricted Eulerian dynamics (Vieillefosse, 1984; Cantwell, 1992; Chacín and Cantwell, 2000), direct numerical simulation (DNS) analysis (Chen *et al.*, 1990; Soria *et al.*, 1994; Martin, 1998; Ooi *et al.*, 1999; Chong *et al.*, 1998), and recent *a priori* LES studies (Borue and Orszag, 1998; van der Bos *et al.*, 2002).

The tensorial invariants of the velocity gradient are essential for understanding small-scale turbulent motions, and there are several good reasons to investigate them: (i) the topological structures obtained from the analysis are universal, viz. frame invariant under affine transformations (Soria *et al.*, 1994; Tsinober, 1998); (ii) in the case of incompressible flows, analysis of a 3-D field can be performed using only two invariants; (iii) different length scales of turbulence corresponding to different magnitudes of the velocity gradient can be sorted in an unambiguous manner using the invariant phase plane; and, (iv) it has been shown in several studies (Blackburn *et al.*, 1996; Chong *et al.*, 1998; Ooi *et al.*, 1999; van der Bos *et al.*, 2002) that the so-called invariant discriminant appears to be an effective quantity for flow structure visualization since it does not require any arbitrary thresholds.

Recently, a dynamic non-linear subgrid-scale (SGS) model (DNM) has been proposed by Wang and Bergstrom (2005). In comparison with the conventional dynamic model (DM) (Germano *et al.*, 1991; Lilly, 1992), the DNM exhibits desirable numerical robustness, flexibility in incorporating backscatter, and a more realistic geometrical representation of the SGS stress, since it allows for more complex alignment pattern between the SGS stress and resolved strain rate tensors. A good SGS model should exhibit the capability to reproduce generic turbulence topological features and also to statistically predict the expected characteristic geometrical alignment patterns between fluid (eigen-)vectors. This paper aims to evaluate the DNM using advanced criteria and explore turbulence topology using the *a posteriori* LES method based on it.

MODEL FORMULATIONS AND PHYSICAL CONCEPTS

Dynamic Non-linear Model

The DNM implemented in this LES approach is based on the quadratic constitutive relation proposed by Speziale and his colleagues (Speziale, 1987; Gatski and Speziale, 1993) for the Reynolds averaged Navier-Stokes (RANS) method, which can be implemented into LES as

$$\begin{cases} \tau_{ij}^* = \tau_{ij} - \tau_{kk}\delta_{ij}/3 = -C_S\beta_{ij} - C_W\gamma_{ij} - C_N\eta_{ij} \\ T_{ij}^* = T_{ij} - T_{kk}\delta_{ij}/3 = -C_S\alpha_{ij} - C_W\lambda_{ij} - C_N\zeta_{ij} \end{cases} \quad (1)$$

where the asterisk is used to indicate a trace-free tensor; τ_{ij} and T_{ij} are the grid-level and test-level SGS stresses, respectively; and C_S, C_W and C_N are model coefficients to be determined dynamically. The tensor quantities appearing in Eq. (1) are defined as

$$\begin{cases} \beta_{ij} = 2\bar{\Delta}^2|\bar{S}|\bar{S}_{ij}, \;\; \gamma_{ij} = 4\bar{\Delta}^2(\bar{S}_{ik}\bar{\Omega}_{kj} + \bar{S}_{jk}\bar{\Omega}_{ki}) \\ \eta_{ij} = 4\bar{\Delta}^2(\bar{S}_{ik}\bar{S}_{kj} - \frac{1}{3}\bar{S}_{mn}\bar{S}_{nm}\delta_{ij}) \\ \alpha_{ij} = 2\tilde{\bar{\Delta}}^2|\tilde{\bar{S}}|\tilde{\bar{S}}_{ij}, \;\; \lambda_{ij} = 4\tilde{\bar{\Delta}}^2(\tilde{\bar{S}}_{ik}\tilde{\bar{\Omega}}_{kj} + \tilde{\bar{S}}_{jk}\tilde{\bar{\Omega}}_{ki}) \\ \zeta_{ij} = 4\tilde{\bar{\Delta}}^2(\tilde{\bar{S}}_{ik}\tilde{\bar{S}}_{kj} - \frac{1}{3}\tilde{\bar{S}}_{mn}\tilde{\bar{S}}_{nm}\delta_{ij}) \end{cases} \quad (2)$$

where $\bar{S}_{ij} = (\bar{u}_{i,j} + \bar{u}_{j,i})/2$ and $\bar{\Omega}_{ij} = (\bar{u}_{i,j} - \bar{u}_{j,i})/2$ are the resolved strain and rotation rate tensors; $|\bar{S}| = (2\bar{S}_{ij}\bar{S}_{ij})^{1/2}$; and $\bar{\Delta}$ and $\tilde{\bar{\Delta}}$ represent the grid and test-grid filter sizes, respectively. The dynamic procedure for obtaining the DNM follows the least-squares approach of Lilly (1992), which results in the following normal equations for determination of

the model coefficients:

$$\begin{bmatrix} M_{ij}M_{ij} & M_{ij}W_{ij} & M_{ij}N_{ij} \\ W_{ij}M_{ij} & W_{ij}W_{ij} & W_{ij}N_{ij} \\ N_{ij}M_{ij} & N_{ij}W_{ij} & N_{ij}N_{ij} \end{bmatrix} \cdot \begin{bmatrix} C_S \\ C_W \\ C_N \end{bmatrix} = - \begin{bmatrix} \mathcal{L}^*_{ij}M_{ij} \\ \mathcal{L}^*_{ij}W_{ij} \\ \mathcal{L}^*_{ij}N_{ij} \end{bmatrix}, \quad (3)$$

where $M_{ij} = \alpha_{ij} - \tilde{\beta}_{ij}$, $W_{ij} = \lambda_{ij} - \tilde{\gamma}_{ij}$, $N_{ij} = \zeta_{ij} - \tilde{\eta}_{ij}$ and $\mathcal{L}^*_{ij}$ is the Leonard term. A detailed derivation of the equation is documented in the paper by Wang and Bergstrom (2005).

Tensorial Invariants and Flow Topologies

The filtered velocity gradient $\bar{A}_{ij} \stackrel{\text{def}}{=} \bar{u}_{i,j}$ can be decomposed into a filtered symmetric strain rate tensor $\bar{S}_{ij}$ and skew-symmetric rotation rate tensor $\bar{\Omega}_{ij}$, as $\bar{A}_{ij} = \bar{S}_{ij} + \bar{\Omega}_{ij}$. The eigenvalues of $\bar{A}_{ij}$ satisfy the *characteristic equation*

$$\lambda^3 + P_{A\Delta}\lambda^2 + Q_{A\Delta}\lambda + R_{A\Delta} = 0, \quad (4)$$

where $P_{A\Delta}$, $Q_{A\Delta}$ and $R_{A\Delta}$ are the invariants of $\bar{A}_{ij}$ which take the following forms for incompressible flow:

$$\begin{cases} P_{A\Delta} = -\bar{A}_{ii} \equiv 0, \\ Q_{A\Delta} = -\frac{1}{2}\bar{A}_{ik}\bar{A}_{ki} = \frac{1}{4}(\bar{\omega}_i\bar{\omega}_i - 2\bar{S}_{ij}\bar{S}_{ji}), \\ R_{A\Delta} = -\frac{1}{3}\bar{A}_{ik}\bar{A}_{kn}\bar{A}_{ni} = -\frac{1}{3}(\bar{S}_{ij}\bar{S}_{jk}\bar{S}_{ki} + \frac{3}{4}\bar{\omega}_i\bar{\omega}_j\bar{S}_{ij}). \end{cases} \quad (5)$$

The tensorial invariants appearing in the above equations are the *resolved enstrophy* $\bar{\omega}^2 = \bar{\omega}_i\bar{\omega}_i = -2\bar{\Omega}_{ij}\bar{\Omega}_{ji}$, *resolved strain product* $\bar{\mathcal{I}}_{S2} = \bar{S}_{ij}\bar{S}_{ji}$, *resolved strain skewness* $\bar{\mathcal{I}}_{S3} = \bar{S}_{ij}\bar{S}_{jk}\bar{S}_{ki}$, and *resolved enstrophy generation* $\bar{\sigma} = \bar{\boldsymbol{\omega}} \cdot \bar{\mathbf{w}} = \bar{\omega}_i\bar{\omega}_j\bar{S}_{ij}$. Here, $\bar{\mathbf{w}}$ is the *resolved vortex stretching vector* defined as $\bar{w}_i = \bar{\omega}_j\bar{S}_{ij}$.

Chong *et al.* (1990) showed that when $P_A = 0$ (due to incompressibility), the nature of the roots of Eq. (4) is determined by a *discriminant* defined as

$$D_A = \tfrac{27}{4}R_A^2 + Q_A^3. \quad (6)$$

If $D_A > 0$, Eq. (4) admits one real and two complex-conjugate roots. In this case, vorticity dominates the rate of strain, the local streamlines swirl about a point and the flow pattern is referred to as a *focus*. If $D_A < 0$, the three roots of Eq. (4) are real and distinct, the rate of strain dominates the vorticity, and the flow pattern resembles a *stagnation point*. This type of flow geometry is referred to as a *node-saddle-saddle*. If $D_A = 0$, Eq. (4) has three real roots of which two are equal, which corresponds to two curves: $R_A = \pm(2\sqrt{3}/9)(-Q_A)^{3/2}$ as shown in Fig. 1. These two special curves are sometimes referred to as the "*Vieillefosse line*" (Chertkov *et al.*, 1999). The sign of R_A can be used for a further classification of the flow topology: in the left half of the Q_A–R_A plane (the so-called *phase plane of invariants* of $\bar{u}_{i,j}$), the real parts of the complex-conjugate eigenvalues or two of the three real eigenvalues are negative and the critical points are classified as *stable*; in contrast, in the right half plane, the real parts of the complex-conjugate eigenvalues or two of the three real eigenvalues are positive and the critical points are classified as *unstable* (Blackburn *et al.*, 1996).

In our presentation of the results that follow, the invariants $Q_{A\Delta}$ and $R_{A\Delta}$ for $\bar{A}_{ij}$ (as well as those for $\bar{S}_{ij}$ to be discussed later) are non-dimensionalized using the wall friction velocity u_τ and kinematic viscosity ν in analogy to the wall coordinate $x_2^+ = x_2 u_\tau/\nu$ for wall flows, i.e.

$$Q^+_{A\Delta} = Q_{A\Delta}/(u_\tau^2/\nu)^2, \quad R^+_{A\Delta} = R_{A\Delta}/(u_\tau^2/\nu)^3. \quad (7)$$

Marginal Expectation of Resolved Quantities

Flow topologies related to the resolved quantities such as enstrophy generation ($\bar{\sigma}$) and the rate of SGS turbulence kinetic energy (TKE) production ($\mathcal{P}_r \stackrel{\text{def}}{=} -\tau^*_{ij}\bar{S}_{ij}$) are investigated. Since these quantities by their nature are scalars, a method is needed to relate them to the invariant phase plane. Following the example of van der Bos *et al.* (2002), we introduce the *marginal expectation* (ME) for a random scalar variable Φ based on its JPDF $P(R_\Delta, Q_\Delta, \phi)$, i.e.

$$\Phi_E = \Phi_E(R_\Delta, Q_\Delta) = \int_\Gamma \phi \cdot P(R_\Delta, Q_\Delta, \phi)d\phi, \quad (8)$$

where Γ is the sample space of Φ with ϕ being the sample-space variable corresponding to Φ. Using Bayes's theorem, the above equation can be re-cast as

$$\Phi_E = P(R_\Delta, Q_\Delta)\langle\Phi|R_\Delta, Q_\Delta\rangle, \quad (9)$$

where $\langle\Phi|R_\Delta, Q_\Delta\rangle = \int_\Gamma \phi P(\phi|R_\Delta, Q_\Delta)d\phi$ is the *conditional expectation* of Φ. As such, the ME of the non-dimensional resolved enstrophy generation $\bar{\sigma}/|\bar{\sigma}| = \cos(\bar{\boldsymbol{\omega}}, \bar{\mathbf{w}})$ is

$$\sigma_E = P(R_\Delta, Q_\Delta) \cdot \langle \cos(\bar{\boldsymbol{\omega}}, \bar{\mathbf{w}}) | R_\Delta, Q_\Delta \rangle ; \quad (10)$$

and the ME for non-dimensionalized $\mathcal{P}_r$ is

$$\mathcal{P}_{rE} = P(R_\Delta, Q_\Delta) \cdot \left\langle \mathcal{P}_r/(u_\tau^4/\nu) | R_\Delta, Q_\Delta \right\rangle . \quad (11)$$

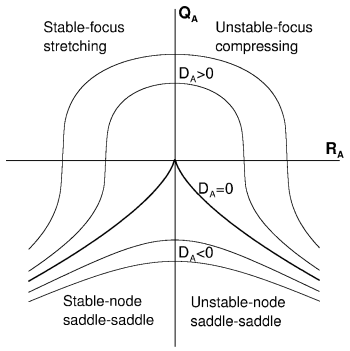

Figure 1: Solution space for invariants Q_A and R_A with curves corresponding to constant values of the discriminant D_A.

RESULTS AND ANALYSIS

In this section, statistical results on turbulence topologies are presented, including illustration of the near-wall anisotropic effect and a report of some new flow phenomenologies discovered using the tensorial invariant phase plane. Numerical simulations were performed for a turbulent Couette flow with a Reynolds number of 2600 (based on one half of the channel width and one half of the velocity difference between the two plates). Details of the numerical simulations can be found in Wang and Bergstrom (2005). In the simulation, 48^3 nodes were used in the discretization of the computational domain and 30×30 bins were used for calculating statistical quantities such as the JPDF of the flow invariants.

Flow Topologies Related to the Invariants of $\bar{\mathbf{A}}_{\mathbf{ij}}$

Figures 2(a)–(d) illustrate the JPDF of $Q_{A\Delta}$ and $R_{A\Delta}$ for the viscous sublayer, buffer zone and logarithmic region. A prototypical *self-similar* "pear-shape" of the JPDF contours [see Fig. 2(b)] is observed in all cases. It is evident from the figures that the most probable state (mode) is located at the origin. Apart from the origin, the 2-D pear-shaped JPDF contours have a preference for the 2nd and 4th quadrants, indicating the prevalence of stable-focus/stretching and unstable-node/saddle/saddle topologies, respectively. From comparison of Figs. 2(a), (c) and (d), it is found that *the preference of the pear-shaped JPDF contour for the origin is the most prominent in the viscous sublayer*, indicating that this

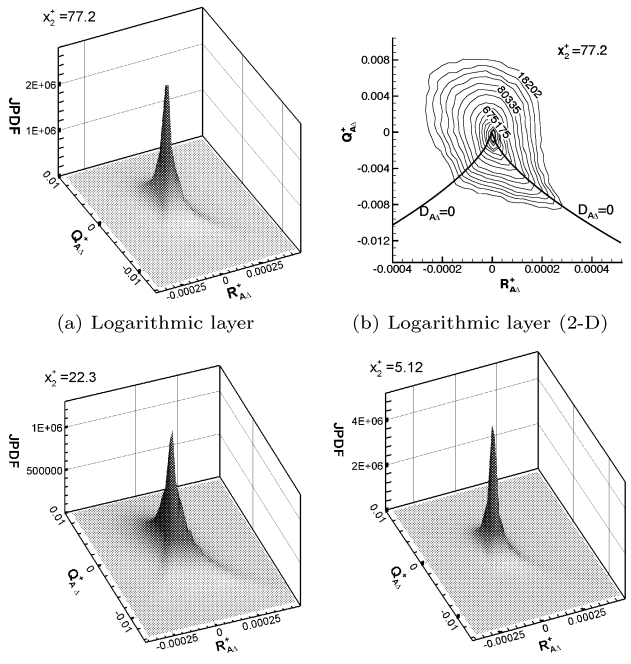

(a) Logarithmic layer (b) Logarithmic layer (2-D)

(c) Buffer layer (d) Viscous sublayer

Figure 2: Contours of JPDF of invariants $Q^+_{A\Delta}$ and $R^+_{A\Delta}$ of the filtered velocity gradient tensor (DNM).

flow signature is not unique for (quasi-)isotropic turbulence as is commonly reported by previous researchers.

As is apparent in the figures, there is a strong tendency for the JPDF contour to gather around the curve ($D_{A\Delta}=0$ for $R_{A\Delta}\geq 0$), forming a so-called "*Vieillefosse tail*" (van der Bos *et al.*, 2002). Similar observations were reported in the *a priori* LES analysis of holographic particle image velocimetry (HPIV) measurements of a square duct flow field by van der Bos *et al.* (2002), various DNS studies of mixing layers by Chen *et al.* (1990) and Soria *et al.* (1994), channel flow by Blackburn *et al.* (1996), turbulent boundary layer flow by Chong *et al.* (1998), stratified homogeneous shear flow by Diamessis and Nomura (2000), homogeneous isotropic turbulent flow by Martin *et al.* (1998), and forced isotropic turbulence by Ooi *et al.* (1999). It is very interesting to note that although the large-scale motions of these flows differ, the statistical features in the $Q_{A\Delta}$–$R_{A\Delta}$ phase plane are similar. This suggests that the topological features shown in the $Q_{A\Delta}$–$R_{A\Delta}$ phase plane are self-similar not only between different layers of a wall-bounded flow, but also between different types of flows as well, which according to Ooi *et al.* (1999) and Martin *et al.* (1998) indicate "a kind of universality for all turbulence flows, be they homogeneous or inhomogeneous".

Flow Topologies Related to the Invariants of $\bar{S}_{ij}$

Clearly, both $Q_{A\Delta}$ and $R_{A\Delta}$ by definition incorporate the combined effects of local straining and vortical rotational processes whose influences are embodied in the four invariants: strain product, strain skewness, enstrophy and enstrophy generation. In their pioneering work, Chen *et al.* (1990) studied flow topology using the invariants of the strain rate tensor, which excludes (in a direct sense) the vorticity information, i.e. enstrophy and enstrophy generation from the set of invariants. As such, the relation between the local flow topology and the straining process is highlighted, which in some cases is advantageous for clarifying flow topologies. The invariants of the filtered strain rate tensor for incompressible flow are:

$$P_{S\Delta}=\bar{S}_{ii}\equiv 0,\ Q_{S\Delta}=-\tfrac{1}{2}\bar{S}_{ik}\bar{S}_{ki},\ R_{S\Delta}=-\tfrac{1}{3}\bar{S}_{ik}\bar{S}_{kn}\bar{S}_{ni}. \quad (12)$$

Clearly, $Q_{S\Delta}$ is a measure of resolved viscous dissipation, i.e.

$$\varepsilon_r = 2\nu\bar{S}_{ij}\bar{S}_{ji}\equiv -4\nu Q_{S\Delta}, \quad (13)$$

and $R_{S\Delta}$ is a measure of the resolved strain skewness, as well as an indicator of the sign of the intermediate eigenvalue of the resolved strain rate tensor, since

$$\bar{\mathcal{I}}_{S3}=\bar{S}_{ik}\bar{S}_{kn}\bar{S}_{ni}\equiv\alpha_S^3+\beta_S^3+\gamma_S^3\equiv 3\alpha_S\beta_S\gamma_S. \quad (14)$$

Here, $\alpha_S\geq\beta_S\geq\gamma_S$ are the three eigenvalues of $\bar{S}_{ij}$ arranged in descending order. Due to continuity, it is clear that $\alpha_S>0$ and $\gamma_S<0$ are valid for any nontrivial situation (the trivial situation refers to $\alpha_S=\beta_S=\gamma_S=0$). Therefore, if $R_{S\Delta}>0$, then $\bar{S}_{ik}\bar{S}_{kn}\bar{S}_{ni}<0$ and $\beta_S>0$, and the local structure is *sheetlike*; on the other hand, if $R_{S\Delta}<0$, $\beta_S<0$, the local structure is *tubelike*. For the most probable ratios of $\alpha_S:\beta_S:\gamma_S=1:1:-2$ (antisymmetric expansion) according to Lund and Rogers (1994) and Tao *et al.* (2002), and $3:1:-4$ according to Ashurst *et al.* (1987) and Tsinober *et al.* (1992), β_S is positively skewed in statistics, which in turn indicates that $R_{S\Delta}$ is positively skewed and the resolved strain skewness is negatively skewed in statistics.

The discriminant for the $Q_{S\Delta}$–$R_{S\Delta}$ phase plane is

$$D_{S\Delta}=\tfrac{27}{4}R^2_{S\Delta}+Q^3_{S\Delta}. \quad (15)$$

Since $\bar{S}_{ij}$ is a real symmetric tensor, all of its three eigenvalues must be real. Therefore, only the region corresponding to $D_{S\Delta}\leq 0$ in the $Q_{S\Delta}$–$R_{S\Delta}$ phase plane is realistic for flow topological classification, which is significantly different than that of the $Q_{A\Delta}$–$R_{A\Delta}$ phase plane. According to Blackburn *et al.* (1996), the $Q_{S\Delta}$–$R_{S\Delta}$ phase plane is very convenient for visualizing the relative eigenvalue ratio of the resolved strain rate tensor. Suppose that $r_a=\beta_S/\alpha_S$, then the curves corresponding to different eigenvalue ratios can be represented by

$$R_{S\Delta}=(-Q_{S\Delta})^{3/2}r_a(1+r_a)(1+r_a+r_a^2)^{-3/2}. \quad (16)$$

Using the above relation, curves corresponding to $\alpha_S:\beta_S:\gamma_S=1:1:2$ (axisymmetric expansion), $2:1:-3$, $3:1:-4$, $1:0:-1$ (2-D flow), $-1:-1:2$ (axisymmetric compression), and the quasi-2-D (QTD) state of flow configuration (related to small r_a) are illustrated in Fig. 3(b).

Figures 3(a)–(d) illustrate both the 3-D and 2-D JPDF contours of the invariants of $\bar{S}_{ij}$. The flow topology in the logarithmic region in both Figs. 3(a) and (b), shows a strong preference for the 4th quadrant ($R_{S\Delta}>0$ and $Q_{S\Delta}<0$), which according to the previous discussion relates to a local dissipative pattern and a positively skewed eigenvalue β_S. A general tendency towards the axisymmetric expansion pattern is observed in Fig. 3(b), especially at low JPDF value levels. As the JPDF value increases, a state with an eigenvalue ratio of $3:1:-4$ becomes more probable. The above method for visualizing the eigenvalue ratio is convenient and intuitive. However, it is argued by the authors that *it is inadequate to establish any quantitative results on the most probable eigenvalue ratio based on the JPDF contour pattern exhibited in the $Q_{S\Delta}$–$R_{S\Delta}$ phase plane.* This is because all states of high probability cluster around the peak location, where the different eigenvalue ratio curves specified by Eq. (16) are hardly distinguishable; whereas, those most distinguishable patterns in the 4th quadrant correspond to lower probabilities.

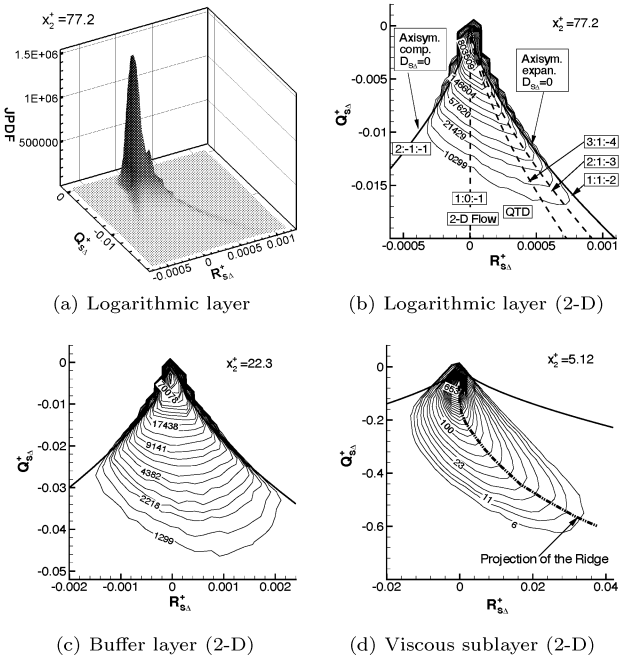

(a) Logarithmic layer (b) Logarithmic layer (2-D)

(c) Buffer layer (2-D) (d) Viscous sublayer (2-D)

Figure 3: Contours of the JPDF of invariants $Q^+_{S\Delta}$ and $R^+_{S\Delta}$ of the filtered strain rate tensor (DNM).

From Figs. 3(b), (c) and (d), it is observed that the most probable state is located near the origin. However, there appears to be a shift of this peak location (mode) away from the origin along the negative $Q_{S\Delta}$ axis. From these three figures, it is observed that this negative shift from the origin increases as the wall is approached, which according to Blackburn *et al.* (1996) is a consequence of the wall anisotropic effect. Right at the wall, the boundary condition for $\bar{S}_{ij}$ results in

$$R_{S\Delta}|_{wall} \equiv 0, \quad Q_{S\Delta}|_{wall} = -\tfrac{1}{4}(\bar{u}^2_{1,2} + \bar{u}^2_{3,2})|_{wall}. \qquad (17)$$

Since $Q_{S\Delta}$ is a direct indicator of local dissipation [see Eq. (13)], the term *near-wall dissipation shift in the $Q_{S\Delta}$–$R_{S\Delta}$ phase plane* is coined here to describe this phenomenon. The value of $R_{S\Delta} \equiv 0$ at the wall helps to explain the special pattern of the projection of the probable 3-D JPDF contour ridge in the $Q_{S\Delta}$–$R_{S\Delta}$ plane (the dash-dot-dot line) shown in Fig. 3(d), which becomes more and more "vertical" (thus more and more 2-D) as the origin is approached. *This observed feature is important, as it demonstrates a generic characteristic of the near-wall flow: namely, in the viscous sublayer the most probable states are close to a 2-D pattern, whereas the two limiting flow configurations, i.e. axisymmetric compression/expansion, are the least probable due to their 3-D physical nature.* It is very encouraging to see such a regular and universal flow topology for the buffer zone in both Figs. 2(c) and 3(c) with the aid of the tensorial invariant phase plane, since the buffer zone is still considered to be one of the most controversial flow regimes in wall-bounded turbulence.

Marginal Expectation of Resolved Enstrophy Generation σ_E

The resolved enstrophy generation is closely related to the process of local vortex stretching/compression and the cascade of kinetic energy dissipation. Research on enstrophy generation using the methodology of turbulence topology includes the works of Chertkov *et al.* (1999) and van der Bos *et al.* (2002), who analyzed (quasi-)isotropic turbulence data based on DNS and HPIV measurements, respectively. Generally speaking, this research methodology which relates turbulence topology to enstrophy generation is still relatively new. In this subsection, we report some interesting phenomenological results on the resolved enstrophy generation and associated flow topologies observed in our research.

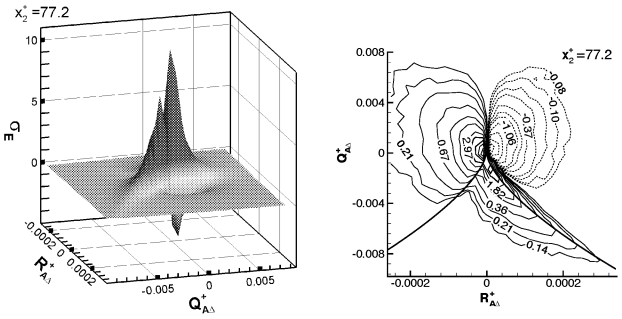

(a) Logarithmic layer (b) Logarithmic layer (2-D)

Figure 4: Marginal expectation of the resolved enstrophy generation σ_E as a function of $Q^+_{A\Delta}$ and $R^+_{A\Delta}$ (DNM). Positive values: solid lines, negative values: dashed lines.

Figures 4(a)–(b) exhibit the contours[1] of the ME of the resolved enstrophy generation σ_E in the $Q_{A\Delta}$–$R_{A\Delta}$ phase plane. From Fig. 4(b), a "dragonfly-shaped" contour is observed in the logarithmic layer, which is similar to the observation of Chertkov *et al.* (1999) and van der Bos *et al.* (2002). The σ_E function in the invariant phase plane has two positive peaks corresponding to a localized vortex stretching configuration. Both positive peaks are close to the origin. The dominant positive peak in the region of $D_{A\Delta} > 0$ and $R_{A\Delta} < 0$ relates to the stable-focus/stretching flow topology, and the secondary positive peak in the 4th quadrant gathers around the right Vieillefosse line ($D_{A\Delta} = 0$). A negative σ_E peak is observed in the region of $D_{A\Delta} > 0$ and $R_{A\Delta} > 0$, which relates to the unstable-focus/compressing topology. In effect, in the buffer and viscous sublayer regions, an additional secondary negative peak can be also observed in the third quadrant (not shown). The predominant positive and negative contours suggestively form the shape of a pair of "eyes" of the "dragonfly", with the secondary positive peak positioned along the Vieillefosse tail forming its "body".

Figures 5(a)–(f) show the contours of σ_E in the invariant phase plane of $\bar{S}_{ij}$ (i.e., $Q_{S\Delta}$–$R_{S\Delta}$ phase plane), which displays a very interesting *pattern of a pair of "wings"*: a negative wing located in the region of $D_{S\Delta} < 0$ and $R_{S\Delta} < 0$, and a positive wing located in the region of $D_{S\Delta} < 0$ and $R_{S\Delta} > 0$. The three characteristic limiting curves that separate and confine the two wings correspond to: the left Vieillefosse line $D_{S\Delta} = 0$ (axisymmetric compression), $R^+_{S\Delta} = 0$ (2-D flow), and the right Vieillefosse line $D_{S\Delta} = 0$ (axisymmetric expansion). As shown in Figs. 5(a) and (b), in the logarithmic region, the positive peak dominates the negative one; also, the positive wing contour has a strong tendency toward the right Vieillefosse line which relates to axisymmetric expansion, whereas, the negative wing shows a weak preference toward the left Vieillefosse line which links to axisymmetric compres-

[1]The contour levels of the ME of the various flow quantities shown in Figs. 4–8 have been magnified by a factor of 30×30.

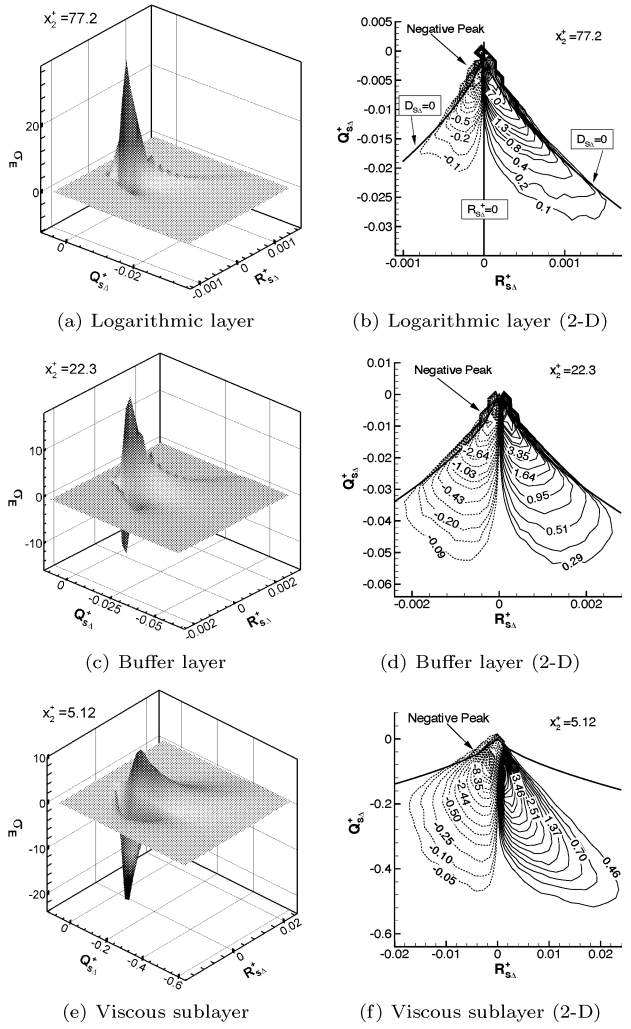

(a) Logarithmic layer (b) Logarithmic layer (2-D)

(c) Buffer layer (d) Buffer layer (2-D)

(e) Viscous sublayer (f) Viscous sublayer (2-D)

Figure 5: Marginal expectation of the resolved enstrophy generation σ_E as a function of $Q^+_{S\Delta}$ and $R^+_{S\Delta}$ (DNM). Positive values: solid lines, negative values: dashed lines.

sion. Figs. 5(c) and (d) show that in the buffer region, the negative and positive peaks are about the same magnitude and therefore the two wings are more symmetric. No obvious preferential topological state associated with σ_E is observed in the buffer zone. From Figs. 5(e) and (f), it is clear that in the viscous sublayer, the negative peak becomes dominant, and both wings move closer to the central 2-D line ($R^+_{S\Delta}=0$). *This phenomenological observation is interesting since it indicates the 2-D nature of the viscous sublayer, where the local vortex compressing flow configuration is dominant and the influence of the limiting 3-D axisymmetric expansion and compression flow configurations on σ_E is negligible.*

Marginal Expectation of the SGS TKE Production Rate $\mathcal{P}_{rE}$

van der Bos *et al.* (2002) proposed an interesting statistical technique for visualizing the forward and backward scatters of SGS TKE flux using the invariant phase plane. The ME for the forward scatter and backward scatter of non-dimensionalized SGS TKE (denoted as $\mathcal{P}^+_{rE}$ and $\mathcal{P}^-_{rE}$, respectively) can be defined by splitting Eq. (11) into two parts according to the sign of $\mathcal{P}_r$, i.e. $\mathcal{P}_{rE}=\mathcal{P}^+_{rE}+\mathcal{P}^-_{rE}$, with

$$\begin{cases} \mathcal{P}^+_{rE} \overset{\text{def}}{=} P(R_\Delta,Q_\Delta)\cdot\langle \mathcal{P}_r/(u_\tau^4/\nu)|R_\Delta,Q_\Delta,\mathcal{P}_r>0\rangle \\ \mathcal{P}^-_{rE} \overset{\text{def}}{=} P(R_\Delta,Q_\Delta)\cdot\langle \mathcal{P}_r/(u_\tau^4/\nu)|R_\Delta,Q_\Delta,\mathcal{P}_r<0\rangle. \end{cases} \quad (18)$$

Figures 6(a) and (b) show the net forward and backward scatters of SGS TKE in the logarithmic region, respectively. Both the $\mathcal{P}^+_{rE}$ and $\mathcal{P}^-_{rE}$ contours show a pear-shaped pattern and strong tendency to follow the right Vieillefosse lines of $D_{A\Delta}=0$. By comparing the peak values shown in Figs. 6(a) and (b), it is concluded that the overall SGS TKE transfer is positive, indicating a net forward scatter of TKE from the filtered to the subgrid scales. From both figures, it clear that the effect of backscatter predicted by the DNM is significant. Fig. 7 shows the 2-D contours of $\mathcal{P}^+_{rE}$ and $\mathcal{P}^-_{rE}$. A preference for the right Vieillefosse line of $D_{S\Delta}=0$ is evident, which relates to the local axisymmetric expansion flow configuration. Fig. 8 illustrates the contours of $\mathcal{P}^+_{rE}$ predicted by the DM, which is different than those predicted using the DNM. For the DM, the principal axes of the SGS stress tensor are strictly aligned with those of the resolved strain rate tensor; consequently, no net backscatter could be observed (i.e., $\mathcal{P}^-_{rE}=0$). Since no net backscatter effect is involved, the peak value predicted by the DM in Fig. 8 is, as expected, smaller than that predicted using the DNM shown in Fig. 6(a).

CONCLUSIONS

Turbulence flow topologies predicted by the DNM SGS model are compared with those predicted by the conventional DM, and reported results based on DNS and experimental data analysis. It is concluded that within the logarithmic region (away from the walls), the DNM can successfully predict prototypical flow topologies such as the pear-shaped JPDF contour of the invariants of the velocity gradient tensor. It is observed that the influence of the near-wall anisotropy on the flow topologies is significant. For instance, the preference of the pear-shaped JPDF contour for the origin is found to be the most prominent in the viscous sublayer, indicating that this flow signature is not unique for (quasi-)isotropic turbulence as it is commonly reported in the literature. A negative shift of the JPDF peak location is observed in the $Q_{S\Delta}$–$R_{S\Delta}$ phase plane, a feature that is shown to be linked directly to the wall dissipation through a boundary condition of the invariant at the wall, viz. $Q_{S\Delta}|_{wall}=-(\bar{u}^2_{1,2}+\bar{u}^2_{3,2})|_{wall}/4$.

In the $Q_{A\Delta}$–$R_{A\Delta}$ phase plane for the logarithmic region, the marginal expectation (ME) of resolved enstrophy generation σ_E has two positive peaks, both close to the origin,

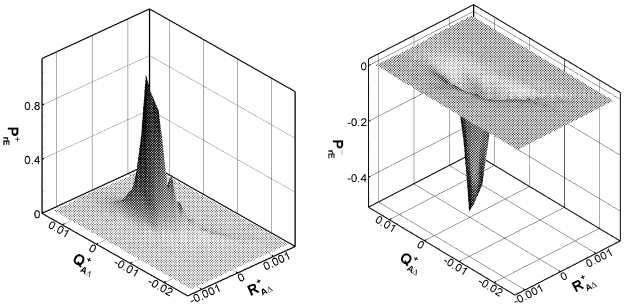

(a) Forward scatter (b) Backscatter

Figure 6: Marginal expectation $\mathcal{P}_{rE}$ in the $Q_{A\Delta}$–$R_{A\Delta}$ phase plane for $x_2^+=77.2$ (DNM).

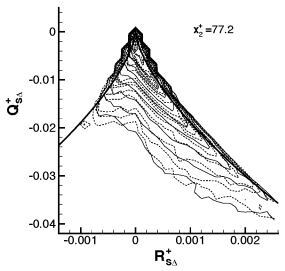

Figure 7: Marginal expectation $\mathcal{P}_{rE}$ in the logarithmic region (DNM).

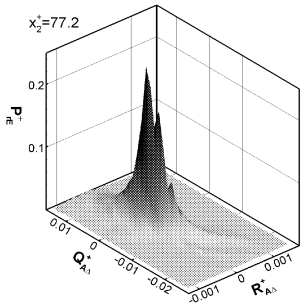

Figure 8: Marginal expectation $\mathcal{P}_{rE}$ in the logarithmic region (DM).

demonstrating a 2-D "dragonfly-shaped" pattern. The predominant positive peak is located in the region of $D_{A\Delta} > 0$ and $R_{A\Delta} < 0$ and is related to a stable-focus/stretching flow topology. The region of $D_{A\Delta} > 0$ and $R_{A\Delta} > 0$ relates to an unstable-focus/compressing topology and is characterized by a negative σ_E peak. In the $Q_{S\Delta}$–$R_{S\Delta}$ phase plane, we discovered that the σ_E contours exhibit the shape of a pair of "wings": the negative and positive contours are confined by three characteristic curves; namely, the left Vieillefosse line $D_{S\Delta} = 0$ (axisymmetric compression pattern), $R_{S\Delta} = 0$ (2-D flow pattern), and the right Vieillefosse line $D_{S\Delta} = 0$ (axisymmetric expansion pattern). In the viscous sublayer, the negative σ_E peak becomes dominant and both wings approach closer to the 2-D line ($R_{S\Delta} = 0$) moving away from both the left and right limiting Vieillefosse lines, reflecting the generic 2-D nature of near-wall flow.

The predicted ME for the forward and backward scatters of SGS TKE fluxes using the DNM are examined separately. In the logarithmic region, the ME contours of the net forward and net backward scatters exhibit a pear-shaped pattern and a strong tendency to follow the right Vieillefosse line ($D_{S\Delta} = 0$ for $R_{S\Delta} > 0$), indicating that the SGS TKE flux is preferentially associated with the axisymmetric expansion flow configuration. The conventional DM fails to predict backscatter in the tensorial invariant plane, and as expected, the peak value of the forward scatter predicted by the DM is smaller than that predicted using the DNM.

REFERENCES

Ashurst, Wm. T., Kerstein, A. R., Kerr, R. M., and Gibson, C. H., 1987, "Alignment of Vorticity and Scalar Gradient with Strain Rate in Simulated Navier-Stokes Turbulence", *Phys. Fluids*, Vol. 30, pp. 2343–2353.

Blackburn, H. M., Mansour, N. N., and Cantwell, B. J., 1996, "Topology of fine-scale motions in turbulent channel flow", *J. Fluid Mech.*, Vol. 310, pp. 269-292.

Borue, V. and Orszag, S. A., 1998, "Local energy flux and subgrid-scale statistics in three dimensional turbulence", *J. Fluid Mech.*, Vol. 366, pp. 1-31.

Cantwell, B. J., 1992, "Exact solution of a restricted Euler equation for the velocity gradient tensor", *Phys. Fluids A*, Vol. 4, pp. 782-793.

Chacín, J. M. and Cantwell, B. J., 2000, "Dynamics of a low Reynolds number turbulent boundary layer", *J. Fluid Mech.*, Vol. 404, pp. 87-115.

Chen, J. H., Chong, M. S., Soria, J., Sondergaard, R., Perry, A. E., Rogers, M., Moser, R., and Cantwell, B. J., 1990, "A study of the topology of dissipating motions in direct numerical simulations of time-developing compressible and incompressible mixing layers", *Proc. CTR Summer Program*, Stanford Univ., pp. 139-164.

Chertkov, M., Pumir, A., and Shraiman, B. I., 1999, "Lagrangian tetrad dynamics and the phenomenology of turbulence", *Phys. Fluids*, Vol. 11, pp. 2394-2410.

Chong, M. S., Perry, A. E., and Cantwell, B. J., 1990, "A general classification of three-dimensional flow fields", *Phys. Fluids A*, Vol. 2, pp. 765-777.

Chong, M. S., Soria, J., Perry, A. E., Chacín, J., Cantwell, B. J., and Na, Y., 1998, "Turbulence structures of wall-bounded shear flows found using DNS data", *J. Fluid Mech.*, Vol. 357, pp. 225-247.

Diamessis, P. J. and Nomura, K. K., 2000, "Interaction of vorticity, rate-of-strain, and scalar gradient in stratified homogeneous sheared turbulence", *Phys. Fluids*, Vol. 12, pp. 1166–1188.

Gatski T. B. and Speziale C. G., 1993, "On explicit algebraic stress models for complex turbulent flows", *J. Fluid Mech.*, Vol. 254, pp. 59-78.

Germano, M., Piomelli, U., Moin, P., and Cabot, W. H., 1991, "A Dynamic Subgrid-Scale Eddy Viscosity Model", *Phys. Fluids A*, Vol. 3, pp. 1760–1765.

Lilly, D. K., 1992, "A proposed modification of the Germano subgrid-scale closure method", *Phys. Fluids A*, Vol. 4, pp. 633-635.

Lund, T. S. and Rogers, M. M., 1994 "An Improved Measure of Strain State Probability in Turbulent Flows", *Phys. Fluids*, Vol. 6, pp. 1838–1847.

Martín, J., Ooi, A., Chong, M. S., and Soria, J., 1998, "Dynamics of the velocity gradient tensor invariants in isotropic turbulence", *Phys. Fluids*, Vol. 10, pp. 2336-2346.

Ooi, A., Martín, J., Soria, J., and Chong M. S., 1999, "A study of the evolution and characteristics of the invariants of the velocity-gradient tensor in isotropic turbulence", *J. Fluid Mech.*, Vol. 381, pp. 141-174.

Perry, A. E. and Chong, M. S., 1987., "A description of eddying motions and flow patterns using critical-point concepts", *Ann. Rev. Fluid Mech.*, Vol. 19, pp. 125-155.

Soria, J., Sondergaard, R., Cantwell, B. J., Chong, M. S., and Perry, A. E., 1994, "A study of the fine-scale motions of incompressible time-developing mixing layers", *Phys. Fluids*, Vol. 6, pp. 871-884.

Speziale, C. G., 1987, "On nonlinear k-l and k-ϵ models of turbulence", *J. Fluid Mech.*, Vol. 178, pp. 459-475.

Tao, B., Katz, J., and Meneveau, C., 2002, "Statistical geometry of subgrid-scale stresses determined from holographic particle image velocimetry measurements", *J. Fluid Mech.*, Vol. 457, pp. 35-78.

Tsinober, A., 1998, "Is concentrated vorticity that important?", *Eur. J. Mech. B/Fluids*, Vol. 17 , pp. 421-449.

van der Bos, F., Tao, B., Meneveau, C., and Katz, J., 2002, "Effects of small-scale turbulent motions on the filtered velocity gradient tensor as deduced from holographic particle image velocimetry measurements. *Phys. Fluids*, Vol. 14, pp. 2456-2474.

Vieillefosse, P., 1984, "Internal motion of a small element of fluid in an inviscid flow", *Physica A*, Vol. 125, pp. 150-162.

Wang B.-C. and Bergstrom D. J., 2005, "A dynamic nonlinear subgrid-scale stress model", *Phys. Fluids*, Vol. 17, pp. 035109:1-15.